14 (2022) 100093

Contents lists available at ScienceDirect

Journal of Non-Crystalline Solids: X

journal homepage: www.sciencedirect.com/journal/journal-of-non-crystalline-solids-x

Internal nucleation tendency and crystal surface energy obtained from bond energies and crystal lattice data

C. Tielemann [a], S. Reinsch [a], R. Maaß [a,b], J. Deubener [c], R. Müller [a,*]

[a] Federal Institute for Materials Research and Testing (BAM), Unter den Eichen 87, 12205 Berlin, Germany
[b] Department of Materials Science and Engineering, University of Illinois at Urbana-Champaign, Urbana, IL 61801, USA
[c] Clausthal University of Technology, Institute of Non-Metallic Materials, Zehntnerstr. 2A, 38678 Clausthal-Zellerfeld, Germany

ARTICLE INFO

Keywords:
Glass
Nucleation tendency
Fracture surface energy
Crystal lattice
Bond energy

ABSTRACT

We present an easy-to-apply method to predict structural trends in the internal nucleation tendency of oxide glasses. The approach is based on calculated crystal fracture surface energies derived from easily accessible diatomic bond energy and crystal lattice data. The applicability of the method is demonstrated on literature nucleation data for isochemically crystallizing oxide glasses.

1. Introduction

One preferred option to synergistically exploit the best properties from both crystalline and amorphous solids is their co-existence in one and the same material. Examples of such materials are glass-ceramics that are known for their exceptional properties. Key to this technology is the understanding of how crystal nucleation and growth can be controlled [1] and, more specifically, how dense internal nucleation can be achieved upon heating [2].

A high crystal number density in the glass interior is frequently achieved by introducing external (foreign) nucleation sites as so-called nucleation agents or seed formers. In the absence of such sites, the driving force for crystal nucleation becomes crucial for dense internal nucleation although gases or materials for handling can still provide external sites for heterogeneous surface nucleation [3,4]. Predicting the internal homogeneous nucleation tendency is also important for the general understanding the glass-forming ability of super cooled liquids and the thermal stability of their glasses.

A widely known approach in predicting the internal nucleation tendency is based on experimental glass transition and crystal melting temperature data, T_g and T_m [5–10]. Within this approach, the driving force of crystal nucleation in glass-forming liquids scales with T_g/T_m where $T_g/T_m < 0.58$ indicates dominant internal nucleation. The approach utilizes that, in practice, the homogeneous nucleation rate, I_0, reaches its maximum, I_{max}, close to T_g for internal nucleation in seed former-free systems and that $\log(I_{max})$ decreases linearly with the increase of T_g/T_m. It was also shown that scaling I_0 with T_g/T_m is, of course, limited by the experimental detection limit, which is $\approx 10^{-8}$ $mm^{-3}\,s^{-1}$ for a reasonable sample size and dwell time, and that $T_g/T_m = 0.58$ corresponds with this threshold [6].

Apart from this concept, however, it remains until today a challenge to predict if a given glass will show dense internal nucleation; even if one considers only seed former-free systems and so-called isochemical transitions where the chemical composition of the parent glass and the evolving crystal are the same. In this context, it has repeatedly been shown that structural similarities between the crystal and the parent glass in terms of density [11] [10], configurational entropy [12], or frozen-in birefringence [13] favor the internal nucleation tendency.

Based on classical nucleation theory, however, I_0 is expected to strongly correlate with the crystal-melt interfacial energy, γ_{CM}. Ideally, this quantity should therefore be used to predict I_0. However, despite many attempts to approximate its magnitude [14–19], γ_{CM} remains experimentally inaccessible.

On the other hand, a previous study [20] showed that the crystal fracture surface energy, γ_{CV}, yielded valuable hints on how γ_{CM} depends on crystal structure. In this study, the orientation of crystals grown from the surface of heated glass samples could be explained in terms of calculated γ_{CV} data assuming that the crystal surface is dominated by low-indexed lattice planes representing minimum energy cuts through the crystal structure. This latter idea is in line with the earlier postulation of Rouxel and co-workers [21] that propagating cracks do always prefer the path of breaking the weakest bonds available.

* Corresponding author.
E-mail address: ralf.mueller@bam.de (R. Müller).

https://doi.org/10.1016/j.nocx.2022.100093
Received 8 February 2022; Received in revised form 25 March 2022; Accepted 4 April 2022
Available online 6 April 2022

Adopting this approach, we propose that γ_{CV} can also be used to predict structural trends in the internal crystal nucleation tendency. Therefore, γ_{CV} is calculated from bond energy and crystal lattice data for a variety of crystals growing in their isochemical glass-forming melt and compared with their nucleation behavior.

2. Theory

The evolving crystal surface is assumed to be equally dominated by the low indexed lattice planes (100), (010) and (001). Then, for the mean crystal fracture surface energy one has:

$$\gamma_{CV} \approx \frac{\left(\gamma_{(100)} + \gamma_{(010)} + \gamma_{(001)}\right)}{3} \tag{1}$$

with $\gamma_{(hkl)}$ = planar energy density of the surface parallel to the lattice plane (*hkl*). It is further assumed that the crystal surface is the one with the lowest possible surface energy with this orientation.

Fig. 1 exemplarily illustrates minimum energy cuts through the fresnoite crystal structure of stoichiometry $Ba_2(TiO)[Si_2O_7]$ (in oxides = $2BaO{\cdot}TiO_2{\cdot}2SiO_2$, or shortly Ba_2TS_2). For this silicate crystal, layers of mixed SiO_4-tetrahedra and TiO_5-pyramids are stacked along the c-axis and are separated by Ba-O ionic bonds [22]. Due to the lower Ba-O bond energy (Table 1), the minimum energy cut parallel to the (001) lattice planes are located between barium cations and those oxygen atoms building the top of the Si/Ti-polyhedral layer (see orange line in Fig. 1 left). Fig. 1 also indicates that minimum cuts parallel to (100) and (010) lattice planes must slice Ba-O and Ti-O bonds.

The planar energy density of each cut surface is given by:

$$\gamma_{(hkl)} = \frac{1}{N_a}\sum_i \frac{s_{i\ (hkl)}\, U_i}{A_{(hkl)}} \tag{2}$$

where N_a is Avogadro's constant, $A_{(hkl)}$ is the (*hkl*) surface area of the unit cell, *i* refers to the metal cation M_i, $S_{i(hkl)}$ is the number of broken cation-oxygen bonds M_i-O in $A_{(hkl)}$ and U_i is their bond energy. $A_{(hkl)}$ is calculated from the crystal structure data listed in Table 2. U_i is calculated from the diatomic bond energy of monoxides, D_i^0, taken from [23]:

$$U_i = \frac{yi/xi}{CN_i} D_i^0 \tag{3}$$

Table 1
Molar diatomic bond energy for different monoxides D^0 [23], oxygen coordination number (*CN*), oxygen to metal-cation ratio (y/x) of the constituting oxide (M_xO_y), and respective energy of one mole of single M-O bonds (*U*).

M	D^0 (kJ mol^{-1})	*CN*	*y/x*	*U* (kJ mol^{-1})
B	808.9	3	3/2	404
Si	799	4	2/1	400
Ge	659.4	4	2/1	329
Ti	672.4	5	2/1	269
Al	511	4	3/2	192
Sr	426.3	6	1	71
Ba	561.9	8	1	70
Ca	402.1	6	1	67
Pb	382	6	1	63.6
Mg	363.2	6	1	60.5
Li	333.5	4	1/2	41.7
Na	256.1	5	1/2	25.6
K	277.8	6	1/2	23.1

y_i/x_i represents the stoichiometric oxygen to metal-cation ratio available for M_i bonding and was taken from the respective ratio of the constituting oxide components, $M_{ix}O_y$, such as BaO, TiO_2 or SiO_2. CN_i in Eq. 3 represents the M_i-O coordination number. Eq. 3 thus assumes that the bond energy is equally distributed within the coordination polyhedron as a first approximation, although bond-valence bond-length correlations are generally accepted to determine the saturation of cation valence in inorganic crystals (all neighboring cation-anion distances are considered to be bonds although not all of equal strength [24]). Cations in different coordination environments are weighed according to their structure site fractions.

For the tetragonal fresnoite crystal (Fig. 1), the unit cell parameters are $a_0 = 852$ pm and $c_0 = 521$ pm, yielding unit cell surface areas $A_{(001)} = 0.726$ nm^2 and $A_{(100)} = A_{(010)} = 0.444$ nm^2. Parallel to (001), 4 Ba cations are separated per unit cell from non-bridging oxygen of SiO_4-tetrahedra. Fig. 1 shows that each Ba cation is 3-fold coordinated to non-bridging oxygen and, thus, 12 Ba-O bonds are broken. Parallel to (100), 6 Ba-O bonds are broken: 4 at the bottom and 2 at the top of the TiO_5-pyramid, but also 2 Ti-O bonds are affected. Due to the tetragonal symmetry, the surface parallel to (010) can be equally treated. For each breakage of a M_i-O bond, U_i is taken from Table 1. For the fresnoite crystal, one obtains:

$$\gamma_{CV} = \frac{1}{3}\left(2\frac{6\times 70 + 2\times 269}{0.444}\frac{kJ\ mol^{-1}}{nm^2} + \frac{12\times 70}{0.726}\frac{kJ\ mol^{-1}}{nm^2}\right)\frac{1}{6.023\times 10^{23}\ mol^{-1}} = 3.03\frac{J}{m^2} \tag{4}$$

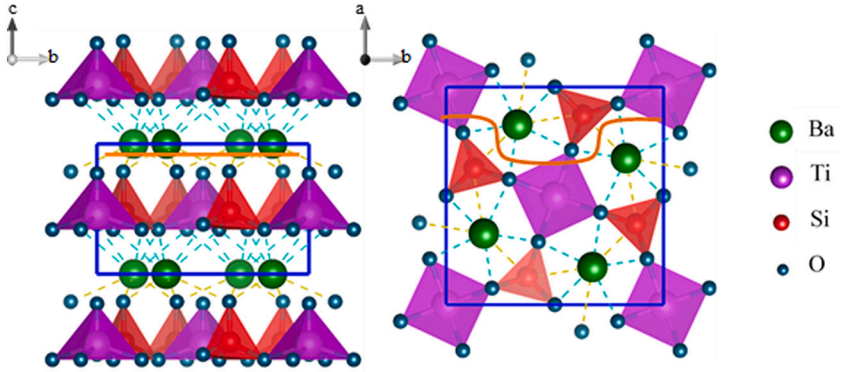

Fig. 1. View on the (100) (left part) and (001) (right part) lattice planes of the fresnoite crystal structure according to [22]. Minimum energy cut surfaces are indicated by orange lines. The blue box shows the unit cell containing two units of formula $Ba_2(TiO)[Si_2O_7]$. (For interpretation of the references to colour in this figure legend, the reader is referred to the web version of this article.)

Table 2
Nominal composition (short oxide formula), transformation temperature (T_g) and nucleation mechanism of glasses undergoing isochemical crystallization (internal = *b*, surface = *s*). Corresponding isochemical crystal (name), oxygen coordination numbers of constituting cations (*CN*), mean crystal fracture surface energy (γ_{CV}) according to Eq. 1–3, and melting point (T_m) are also shown.

Glass			Crystal			
Composition	T_g (K)	Nucleation mechanism	Name [lattice data source]	*CN*	γ_{CV} (Jm^{-2})	T_m (K)
S	1493 [11]	s [26]	High-quartz (S_{HQ}) [27]	4	5.3	1996 [28]
S	1493 [11]	s [26]	High-cristobalite (S_{HC}) [29]	4	5.2	1996 [28]
$M_2A_2S_5$	1088 [30] [31]	s [32]	Quartz-ss# [33]	2/4/4	4.7	1740 [31]
B	523 [28]	s [10]	Boron oxide [34]	3	3.9	723 [28]
$BaAS_2$	1198 [35]	s [35]	Hexacelsian [36]	6/4/4	3.9	2033 [35]
$BaM_2A_3S_9$	1113 [37]	s [38]	Ba-Osumilite [38]	12/6/4/4	3.5	1643 [39]
B_5S_8	970 [40]	b [40]	Barium Silicate [41]	6–8/4	2.9	1719 [42]
BS_2	962 [43]	b [11]	Sanbornite [44]	9/4	2.9	1693 [43]
MCS_2	995 [45]	s [45]	Diopside [46]	8/6/4	2.8	1664 [45]
$M_2A_2S_5$	1088 [45]	s [32]	Cordierite [47]	6/4/4	3.2	1740 [31]
Ba_2TS_2	981 [48]	b [49]*	Fresnoite [22]	8/5/4	3.0	1713 [48]
NAS_6	966 [11]	s [11]	Albite [50]	5/4/4	2.5	1380 [11]
CAS_2	1116 [11]	s [10]**	Anorthite [51]	6–7/4/4	2.4	1826 [11]
NS_2	714 [12]	s [11]	Na-disilicate [52]	5–6/4	2.3	1147 [53]
CS	1030 [54]	b [54]	Wollastonite [55]	8/4	2.1	1817 [56]
KS_2	765 [12]	s [12]	K-disilicate [57]	6–8/4	2.1	1309 [53]
PS	708 [58]	s [58]	Alamosite [59]	5–6/4	2.1	1037 [58]
LS	698 [12]	b [10,12]	Li-metasilicate [60]	5/4	2.0	1474 [61]
LS_2	727 [12]	b [12]	Li-disilicate [62]	4/4	1.9	1307 [61]
NS	661 [12]	b [12]	Na-metasilicate [52]	5/4	1.4	1362 [61]

Keys: References are indicated in brackets, # quartz solid solution with cordierite composition, *often reported to show demixing during the crystallization process, ** borderline case with very small internal nucleation [10]. Nominal compositions: S: SiO_2, $M_2A_2S_5$: $2MgO{\cdot}2Al_2O_3{\cdot}5SiO_2$, B: B_2O_3, $BaAS_2$: $BaO{\cdot}Al_2O_3{\cdot}2SiO_2$, $BaM_2A_3S_9$: $BaO{\cdot}2MgO{\cdot}3Al_2O_3{\cdot}9SiO_2$, BS_2: $BaO{\cdot}2SiO_2$, MCS_2: $MgO{\cdot}CaO{\cdot}2SiO_2$, Ba_2TS_2: $2BaO{\cdot}TiO_2{\cdot}2SiO_2$, NAS_6: $Na_2O{\cdot}Al_2O_3{\cdot}6SiO_2$, CAS_2: $CaO{\cdot}Al_2O_3{\cdot}2SiO_2$, NS_2: $Na_2O{\cdot}2SiO_2$, CS: $CaO{\cdot}SiO_2$, KS_2: $K_2O{\cdot}2SiO_2$, PS: $PbO{\cdot}SiO_2$, LS: $Li_2O{\cdot}SiO_2$, LS_2: $Li_2O{\cdot}2SiO_2$, NS: $Na_2O{\cdot}SiO_2$: B_5S_8: $5BaO{\cdot}8SiO_2$

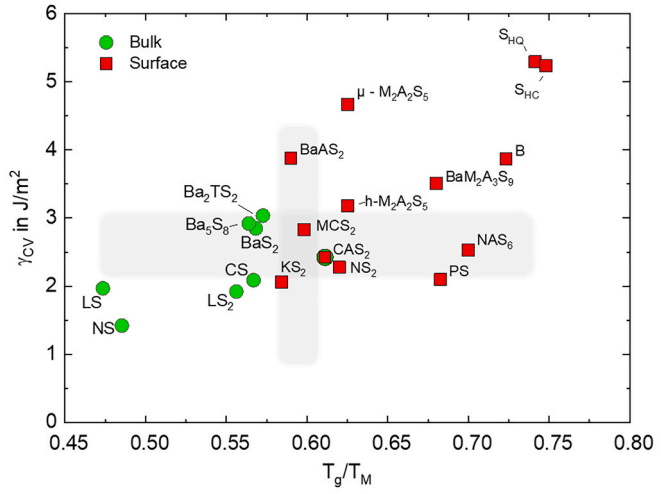

Fig. 2. Oxide glasses isochemically crystallizing via internal (green dots) or surface nucleation (red squares) presented versus T_g/T_M (abscissa) and γ_{CV} (ordinate). Labels show the short oxide formula of the crystal and its isochemical parent glass melt. See Table 2 caption for nominal compositions. The diffuse vertical bar indicates the range of T_g/T_M at ≈ 0.58 above which the internal nucleation rate is not detectable under reasonable experimental conditions and surface nucleation therefore dominates. The diffuse horizontal bar indicates the respective transition range of γ_{CV}. (For interpretation of the references to colour in this figure legend, the reader is referred to the web version of this article.)

3. Results

To emphasize that γ_{CV} can be used to predict internal crystal nucleation tendency, calculations as explained above were performed for a variety of crystals using the crystal structure models provided by VESTA [25] (Table 2).

Fig. 2. shows these calculated γ_{CV} data on its ordinate for these crystals. The nucleation mechanism experimentally observed for these crystals in their isochemical melt is indicated by different symbols. Green dots stand for internal nucleation and red squares for surface nucleation. The horizontal grey bar denotes the overlap range of γ_{CV} for which no clear prediction of nucleation mechanisms seems possible. For $\gamma_{CV} < 2$ and $\gamma_{CV} > 3$ J m^{-2}, however, either internal or only surface induced nucleation has been reported, respectively.

To compare the predictive power of our approach with that of the well-known discrimination via T_g/T_M, all data are presented versus T_g/T_M as well (abscissa). The vertical grey bar indicates the respective overlap range of T_g/T_M, for which both nucleation mechanisms have been observed experimentally.

4. Discussion

Fig. 2 demonstrates that deriving γ_{CV} as a single crystal-based parameter and discriminating via T_g/T_M, reflecting glass and crystal properties, independently allows to roughly predict the mode of crystal nucleation.

The dominance of bulk nucleation in isochemical glass-forming systems for small T_g/T_M is understandable as it indicates that large undercooling is necessary to promote internal nucleation [10]. The correlation between γ_{CV} and the internal nucleation tendency, however, is surprising and not intuitive as the glass fracture surface energy is known to be up to ten times larger than typical glass melt surface energies [63]. Previous work [64] offers insights into this discrepancy, attributing it to the surface enrichment of Na, K, Pb and B due to their low bond energy and high polarizability. Further, preferred orientation of planar BO_3-groups parallel to the melt surface are reported to account for the decrease of the melt surface energy [64].

On the other hand, these relaxation effects indicate that the glass-forming melt can adopt its surface chemistry and structure and it is expected that this remains effective in case of the crystal melt interface as such broken crystal bonds (regardless of the given crystal face) may easily find their structural counterparts in the melt. The adjustment mechanism, which substantially decrease γ_{CM}, however, cannot reach full completeness due to specific volume and entropy differences between melt and crystal. Then, assuming a similar degree of completeness

of this interfacial adjustment at $T > T_g$, the remaining structural and chemical misfits can explain why γ_{CM} scales with γ_{CV}, even though their absolute magnitudes differ significantly.

Such a strong difference is in fact indicated by γ_{CM} data derived from fitting internal nucleation experiments, where γ_{CM} at $\approx T_g$ ranges between 0.068 J/m^2 for N_2CS_3 [65] (0.08 J/m^2 for LS_2 [66]) and 0.31 J/m^2 for N_2CS_3 [67] (0.28 J/m^2 for CS [68]). The direct prove, whether or not these γ_{CM} data scale with γ_{CV}, however, is difficult due to the large scatter of reported γ_{CM} data. γ_{CM} for N_2CS_3 varies over the whole data range between (0.068–0.31 J/m^2) and γ_{CM} for LS_2 scatters between 0.08 J/m^2 [66] and 0.24 J/m^2 [69].

In a recent paper, however, Abyzov et al. [65] could show for γ_{CM} data consistently obtained from nucleation experiments on several stoichiometric glass-forming silicates, that γ_{CM} tends to increase with T_g/T_M. Interestingly, Fig. 2 reveals the same trend for γ_{CV}. This trend might reflect similar structural effects on γ_{CV} and T_g/T_M. In fact, less polymerized crystal structures dominate the lower left corner of Fig. 2 (i.e. small γ_{CV} and T_g/T_M), whereas more polymerized crystals dominate the upper-right corner. This finding seems reasonable, as crystals possessing highly polymerized structures and strong chemical bonds would lead to expect large γ_{CV} as well as a high viscosity (T_g) and T_M values. The degree of structural complexity might even affect T_g/T_M itself. Thus, $T_g/T_M \approx 2/3$ is known as the empirical Beaman-Kauzmann rule for one component glass-forming melts, whereas $T_g/T_M \approx 1/2$ is found for metallic alloys [70].

Whilst such structural trends give some credit to the γ_{CV} data summarized in Fig. 2, the precise values should not be overinterpreted. The large overlap range $\gamma_{CV} \approx$ 2–3 J/m^2 between surface and internal nucleation dominated crystallization might reflect the strong simplifications of our approach and may illustrate given range of uncertainty. In the light of an increasing interest in the bottom-up modeling of glass properties, however, our approach is fundamental as it is based on easily accessible crystal structure and chemical bond energy data and is applicable even for systems where T_g and T_M are not known, difficult to be measured, or modelled.

5. Summary

We derived a method to predict the internal nucleation tendency of oxide glasses. Our approach is based on calculated crystal fracture surface energies derived from diatomic bond energy and crystal lattice data and crystal surfaces. The novel method has been demonstrated on the available set of nucleation data of isochemically crystallizing oxide glasses. This finding indicates that the calculated vacuum fracture energy scales with the crystal-melt interfacial energy, which actually governs the nucleation kinetics. Although the γ_{CV} transition range between surface and internal nucleation dominated glass crystallization is less sharp as that of T_g/T_M, our criterium is accessible even in cases where T_g and T_M are lacking.

CRediT authorship contribution statement

C. Tielemann: Conceptualization, Data curation, Formal analysis, Investigation, Methodology, Software, Validation, Visualization, Writing – original draft, Writing – review & editing. **S. Reinsch:** Conceptualization, Data curation, Funding acquisition, Investigation, Methodology, Project administration, Resources, Supervision, Validation, Writing – review & editing. **R. Maaß:** Resources, Writing – review & editing. **J. Deubener:** Funding acquisition, Validation, Writing – review & editing. **R. Müller:** Conceptualization, Formal analysis, Funding acquisition, Investigation, Methodology, Resources, Supervision, Validation, Visualization, Writing – original draft, Writing – review & editing.

Declaration of Competing Interest

The authors declare that they have no known competing financial interests or personal relationships that could have appeared to influence the work reported in this paper.

Acknowledgement

Support of the Deutsche Forschungsgemeinschaft DFG for the grant (RE 4146/1-1) to S.R. and for the grant (DE 598/31-1) to J.D. is gratefully acknowledged. Further, C.T. thanks M. Nofz of the BAM, Berlin and V. Tonchev of the University of Sofia for valuable remarks.

Appendix A. Supplementary data

Supplementary data to this article can be found online at https://doi.org/10.1016/j.nocx.2022.100093.

References

[1] J. Deubener, M. Allix, M.J. Davis, A. Duran, T. Hoche, T. Honma, T. Komatsu, S. Kruger, I. Mitra, R. Muller, S. Nakane, M.J. Pascual, J.W.P. Schmelzer, E. D. Zanotto, S. Zhou, J. Non-Cryst. Solids 501 (2018) 3.
[2] W. Höland, V. Rheinberger, M. Schweiger, Philosophical transactions of the Royal Society of London, Series A: Mathematical, Physical and Engineering Sciences 361 (2003) 575.
[3] R. Al-Mukadam, J. Deubener, J. Non-Cryst. Solids 524 (2019), 119642.
[4] R. Al-Mukadam, J. Deubener, J. Non-Cryst. Solids 571 (2021), 121068.
[5] D. Turnbull, Contemp. Phys. 10 (1969) 473.
[6] J. Deubener, J. Non-Cryst. Solids 274 (2000) 195.
[7] J. Deubener, Glass Science and Technology-Glastechnische Berichte 73, 2000, p. 178.
[8] V.M. Fokin, E.D. Zanotto, J.W.P. Schmelzer, J. Non-Cryst. Solids 321 (2003) 52.
[9] V.M. Fokin, E.D. Zanotto, N.S. Yuritsyn, J.W.P. Schmelzer, J. Non-Cryst. Solids 352 (2006) 2681.
[10] E. Zanotto, J. Tsuchida, J. Schneider, H. Eckert, Int. Mater. Rev. 60 (2015) 376.
[11] E.D. Zanotto, J. Non-Cryst. Solids 89 (1987) 361.
[12] J. Deubener, Phys. Chem. Glasses 45 (2004) 61.
[13] J. Deubener, F. de Moraes, R. Brückner, J. Non-Cryst. Solids 219 (1997) 57.
[14] R. Becker, Ann. Phys. 424 (1938) 128.
[15] D.R. Cassar, J. Non-Cryst. Solids 511 (2019) 183.
[16] D. Turnbull, J. Appl. Phys. 21 (1950) 1022.
[17] J. Deubener, M. Weinberg, J. Non-Cryst. Solids 231 (1998) 143.
[18] B. Sonderegger, E. Kozeschnik, Metall. Mater. Trans. A 40 (2009) 499.
[19] R. Tran, Z. Xu, B. Radhakrishnan, D. Winston, W. Sun, K.A. Persson, S.P. Ong, Scientific Data 3, 2016, p. 1.
[20] C. Tielemann, R. Busch, S. Reinsch, C. Patzig, T. Höche, I. Avramov, R. Müller, J. Non-Cryst. Solids 562 (2021), 120661, https://doi.org/10.1016/j.jnoncrysol.2021.120661.
[21] T. Rouxel, S. Yoshida, J. Am. Ceram. Soc. 100 (2017) 4374.
[22] P. B. Moore and S. J. Louisnathan, Z. Kristallogr 130 (1969), p. 438.
[23] D.R. Lide, CRC Handbook of Chemistry and Physics, CRC Press, 2004.
[24] I. Brown, D. Altermatt, Acta Crystallogr. Sect. B: Struct. Sci. 41 (1985) 244.
[25] K.M.A.F. Izumi, J. Appl. Crystallogr. 44 (2011) 1272.
[26] R. Brueckner, J. Non-Cryst. Solids 5 (1970) 123.
[27] K. Kihara, Eur. J. Mineral. (1990) 63.
[28] H. Scholze, Glas: Natur, Struktur und Eigenschaften, Springer-Verlag, 2013.
[29] R.W. Wyckoff, Zeitschrift für Kristallographie-Crystalline Materials 62, 1925, p. 189.
[30] R. Müller, R. Naumann, S. Reinsch, Thermochim. Acta 280 (1996) 191.
[31] S. Reinsch, Oberflächenkeimbildung von Silikatgläsern der Stöchiometrie des Cordierits und des Diopsids, TU Berlin, TU-Berlin, 2001.
[32] R. Müller, S. Reinsch, W. Pannhorst, Thermochim. Acta (1996) 280.
[33] K. Langer, W. Schreyer, The American Mineralogist 54, 1969.
[34] S.V. Berger, Acta Chem. Scand. 7 (1953) 611.
[35] W.E. Lee, M. Chen, P.F. James, J. Am. Ceram. Soc. 78 (1995) 2180.
[36] Y. Takeuchi, Mineral. J. 2 (1958) 311.
[37] C. Reich, Herstellung faserverstärkter Glaskeramiken: Optimierung und Charakterisierung mechanischer Eigenschaften, na, 1993.
[38] W. Winter, T. Armbruster, C. Lengauer, Eur. J. Mineral. (1995) 277.
[39] W. Winter, C. Bogdanow, G. Müller, W. Pannhorst, Glastechnische Berichte 66, 1993, p. 109.
[40] X.S. Xia, D.C. Van Hoesen, M.E. McKenzie, R.E. Youngman, K.F. Kelton, Nat. Commun. 12 (2021).
[41] K.F. Hesse, F. Liebau, Zeitschrift fuer Kristallographie 153, 1979, p. 3.
[42] G. Oehlschlegel, Glastechnische Berichte 44, 1971, p. 194.
[43] P. James, J. Non-Cryst. Solids 73 (1985) 517.
[44] M Goreaud, J Choisnet, B Raveau, Deschanvres A : Revue de Chimie Minerale 11 (1974) 207–216.
[45] M.L.F. Nascimento, E.B. Ferreira, E.D. Zanotto, J. Chem. Phys. 121 (2004) 8924.

[46] S. Sasaki, K. Fujino, Y. Takeuchi, R. Sadanaga, Acta Crystal. Sec. A Crystal Phys. Diffraction Theoretical Gen. Crystal. 36 (1980) 904.
[47] K.B. Schwartz, D.B. Leong, R.L. McConville, Phys. Chem. Miner. 20 (1994) 563.
[48] A. Cabral, V. Fokin, E. Zanotto, C. Chinaglia, J. Non-Cryst. Solids 330 (2003) 174.
[49] W. Wisniewski, K. Thieme, C. Rüssel, Prog. Mater. Sci. 98 (2018) 68.
[50] J.K. Winter, F.P. Okamura, S. Ghose, Am. Mineral. 64 (1979) 409.
[51] R.J. Angel, M. Carpenter, L. Finger, Am. Mineral. 75 (1990) 150.
[52] A. Grund, Bulletin de Minéralogie 77 (1954) 775.
[53] K. Takahashi, T. Yoshio, J. Ceram. Soc. Jpn. 81 (1973) 524.
[54] L. Gránásy, T. Wang, P.F. James, J. Chem. Phys. 108 (1998) 7317.
[55] T.M.H. Yamanaka, Acta Crystallographica Section B: Structural Crystallography and Crystal Chemistry 37 (1981) 1010.
[56] B. Phillips, A. Muan, J. Am. Ceram. Soc. 42 (1959) 413.
[57] B. De Jong, H. Super, A. Spek, N. Veldman, G. Nachtegaal, J. Fischer, Acta Crystallogr. Sect. B: Struct. Sci. 54 (1998) 568.
[58] T. Neiman, H. Yinnon, D.R. Uhlmann, J. Non-Cryst. Solids 48 (1982) 393.
[59] S. Krivovichev, P. Burns, Zapiski Vserossijskogo Mineralogicheskogo Obshchestva 133, 2004, p. 70.
[60] H. Seemann, Acta Crystallogr. 9 (1956) 251.
[61] F.C. Kracek, J. Am. Chem. Soc. 61 (1939) 2863.
[62] B. De Jong, P. Slaats, H. Super, N. Veldman, A. Spek, J. Non-Cryst. Solids 176 (1994) 164.
[63] A.K. Varshneya, Fundamentals of Inorganic Glasses, Academic Press, San Diego, 1994.
[64] H. Scholze, Glas - Natur, Struktur und Eigenschaften, Springer-Verlag, Berlin Heidelberg New York, 1988.
[65] A.S. Abyzov, V.M. Fokin, E.D. Zanotto, J. Non-Cryst. Solids 500 (2018) 231.
[66] J. Deubener, Homogene Volumenkeimbildung in Silicatschmelzen: Theorie und Experiment, Fakultät für Prozesswissenschaften, TU Berlin, Berlin, 2001.
[67] N. Diaz-Mora, Cristalização Superficial em Vidros de Cordierita: Morfologia e Cinética, Ph. D. Thesis, DEMa-UFSCar, São Carlos (SP), 1994.
[68] K. Matusita, M. Tashiro, J. Non-Cryst. Solids 11 (1973) 471.
[69] V.M. Fokin, E.D. Zanotto, J. Non-Cryst. Solids 265 (2000) 105.
[70] I. Gutzov, J. Schmelzer, The Vitreous State, Springer, 1995.